Research Square

Preprints are preliminary reports that have not undergone peer review.
They should not be considered conclusive, used to inform clinical practice,
or referenced by the media as validated information.

Geotechnical Enhancement of Marine Clay for Flexible Pavement Subgrade Using Foundry Sand and Alkali-Activated Geopolymers: Experimental Investigation, Machine Learning Prediction

Sai Ram Sangepu

sangepusairam123@gmail.com

Jawaharlal Nehru Technological University, Kakinada

Dr.Koteswara Rao D

Jawaharlal Nehru Technological University, Kakinada

Nitesh Sai pala

Jawaharlal Nehru Technological University, Kakinada

Sugamani Gunta

Indian Institute of Technology Bhubaneswar

Research Article

Keywords: Marine clay, foundry sand, alkali-activated geopolymer, CBR, flexible pavement, linear regression, polynomial regression, Bayesian network, machine learning, IRC:37-2018, VCIC

Posted Date: May 14th, 2026

DOI: https://doi.org/10.21203/rs.3.rs-9380195/v1

License: This work is licensed under a Creative Commons Attribution 4.0 International License.
Read Full License

Additional Declarations: No competing interests reported.

Abstract

Marine clay deposits along the Visakhapatnam–Chennai Industrial Corridor (VCIC), India, present severe challenges for flexible pavement subgrades due to high plasticity, low strength, and high swell potential. This study investigates the stabilisation of marine clay using Foundry Sand (FS) and Alkali-Activated Geopolymer (AAG) through an integrated experimental and data-driven framework. The untreated soil exhibited poor engineering properties (CBR = 1.34%, PI = 40.77%, DFS up to 95%).

Laboratory results identified 10% FS as the optimum mechanical stabiliser, improving compaction and reducing plasticity, but remaining below IRC:37-2018 requirements. The addition of AAG significantly enhanced performance through geopolymerisation. The optimum combination (10% FS + 1.5% AAG) increased CBR to 8.07% (502% improvement), reduced plasticity index by 76.5%, and decreased swell potential by up to 58%. X-ray diffraction (XRD) confirmed mineralogical transformation associated with strength gain.

Regression and machine learning models achieved high predictive accuracy (R^2 up to 0.989), while Bayesian analysis indicated a 94.3% probability of meeting subgrade requirements. Pavement design showed a 28.3% reduction in crust thickness and 33% cost savings. The proposed FS–AAG stabilisation offers a sustainable and cost-effective solution for coastal infrastructure development.

1. Introduction

India's 7,500 km coastline hosts extensive marine clay deposits formed during the Holocene epoch through fluvio-marine sedimentation in deltaic and estuarine environments. Within the Visakhapatnam–Chennai Industrial Corridor (VCIC) a strategically critical economic zone spanning the coastal plains of Andhra Pradesh and Tamil Nadu these deposits are prevalent near Kakinada, Machilipatnam, and the Krishna–Godavari deltaic plains. The VCIC encompasses National Highways, State Expressways, port connectivity roads, and industrial access corridors designed for traffic loads of 50–150 million standard axles (msa). The natural water content of in-situ VCIC marine clays frequently exceeds 100%, and California Bearing Ratio (CBR) values as low as 1.34% make them among the most challenging subgrade materials in Indian highway engineering [1].

Marine clays in this corridor are dominated by montmorillonite and illite clay minerals, conferring high plasticity, poor drainage, significant compressibility, and pronounced swell shrink behaviour under moisture variation [2],[3]. Constructing flexible pavements directly over untreated marine clay requires pavement crust thicknesses exceeding 900 mm, dramatically escalating material consumption and construction cost. Inadequate treatment leads to differential settlement, rutting, pavement cracking, and premature structural failure, disrupting supply chains dependent on VCIC road networks.

Foundry Sand (FS) abundantly generated by metal-casting foundries in East and West Godavari industrial districts comprises high-purity silica-rich, non-plastic granular particles that improve gradation, drainage, and frictional resistance of cohesive clay, reducing plasticity and enhancing compaction characteristics

[5],[6]. Alkali-Activated Geopolymers (AAG) synthesised from NaOH and Na_2SiO_3 solutions form stable cementitious matrices through polycondensation of aluminosilicate phases, substantially enhancing inter-particle bonding, strength, and long-term durability [7],[8]. The combined FS–AAG approach simultaneously addresses mechanical (particle gradation) and chemical (cementitious bonding) deficiencies while diverting two industrial waste streams from landfill.

Despite advances in individual stabilisation methods, predictive frameworks that quantify non-linear interactions between multiple additives and geotechnical responses remain limited. Machine learning (ML) has emerged as a transformative tool in geotechnical engineering, enabling data-driven optimisation of stabiliser dosages [9],[10]. Ensemble models such as Random Forest and Gradient Boosting have demonstrated cross-validated $R^2 > 0.92$ for CBR and compaction property prediction in stabilised soils [11],[12]. Bayesian networks a class of probabilistic graphical models that encode causal dependencies between variables are increasingly applied in geotechnical reliability assessment, offering interpretable uncertainty quantification beyond classical hypothesis testing [13],[14].

Linear and polynomial regression analyses provide explicit mathematical equations relating stabiliser content to geotechnical response, bridging experimental data and deterministic design practice. Multi-variable polynomial response surface models allow joint optimisation of FS and AAG dosages across the complete design space [15].

The present study addresses four specific gaps: (i) no published work reports combined FS–AAG stabilisation of VCIC marine clay under the geochemical conditions prevailing at Kakinada; (ii) Bayesian network modelling and sequential Bayesian inference have not been applied to probabilistic CBR reliability assessment for dual-additive stabilisation; (iii) explicit linear, polynomial, and multi-variable regression equations for FS and AAG effects on all key geotechnical properties have not been reported for this material system; and (iv) IRC:37-2018 pavement design with full economic and environmental analysis has not been conducted for VCIC marine clay. This paper addresses all four gaps through a systematic experimental, statistical regression, Bayesian network, ML prediction, and design framework.

2. Materials

2.1 Marine Clay

Marine clay was collected from a depth of 0.5–1.0 m below ground level from the coastal zone opposite the Coast Guard Station, Kakinada Port, East Godavari District, Andhra Pradesh (16°56'N, 82°14'E), following IS:2720 (Part 1) protocols. Samples were sealed in airtight containers and transported to the geotechnical laboratory. The collected soil exhibited a dark grey colour, strong plasticity on remoulding, and natural moisture content ranging from 82% to 105%, reflecting the highly saturated in-situ state. Geotechnical properties are summarised in Table 1. The soil classifies as CH (high-plasticity inorganic clay) in the Unified Soil Classification System (IS:1498), with clay fraction of 58–67% (< 2 μm), dominated by montmorillonite and illite as confirmed by XRD analysis [1],[2].

Table 1
Geotechnical properties of native Kakinada marine clay.

S.No	Property	Symbol	Value	Standard
1	Specific Gravity	G□	2.25	IS:2720 Pt.3
2	Natural Moisture Content (%)	W	82–105	IS:2720 Pt.3
3	Liquid Limit (%)	WL	70.13	IS:2720 Pt.5
4	Plastic Limit (%)	WP	29.36	IS:2720 Pt.5
5	Plasticity Index (%)	IP	40.77	IS:2720 Pt.5
6	Differential Free Swell (%)	DFS	82–95	IS:2720 Pt.40
7	OMC – Modified Proctor (%)	OMC	30.91	IS:2720 Pt.8
8	Max. Dry Density (kN/m³)	MDD	1.58	IS:2720 Pt.8
9	Soaked CBR (%)	CBR	1.34	IS:2720 Pt.16
10	Cohesion (kN/m²)	c	145.18	IS:2720 Pt.12
11	Angle of Internal Friction (°)	φ	2.56–3.28	IS:2720 Pt.12
12	USCS Classification	–	CH	IS:1498
13	Clay Fraction < 2 μm (%)	–	58–67	IS:2720 Pt.4

2.2 Foundry Sand (FS)

Foundry sand was procured from Sri Bhavani Castings Ltd., Kakinada a ferrous casting foundry employing conventional green sand casting and allied industries at Dhavaleswaram, Rajahmundry. The spent foundry sand (SFS) comprises SiO_2 (87–91%), Al_2O_3, Fe_2O_3, CaO, and MgO. Physical and chemical properties are listed in Table 2. It exhibits mean particle size d_{50} = 0.35 mm, uniformity coefficient C_u = 3.8, curvature coefficient C□ = 1.2, specific gravity Gs = 2.61, non-plastic (NP) Atterberg behaviour, and classifies as SP (poorly-graded sand) in the USCS. Without recycling, large volumes of SFS from the Godavari industrial belt create significant environmental landfill burdens [4],[5].

Table 2
Physical and chemical properties of Foundry Sand (FS).

Property	Value	Property	Value
Specific Gravity	2.61	SiO_2 content (%)	87–91
D_{50} (mm)	0.35	Al_2O_3 (%)	3.2–5.1
Uniformity Coefficient C_u	3.8	Fe_2O_3 (%)	1.8–2.5
Curvature Coefficient C	1.2	CaO (%)	0.5–1.1
USCS Classification	SP	Atterberg Behaviour	Non-plastic
Colour	Dark grey/light brown	Organic content (%)	< 0.5

2.3 Alkali-Activated Geopolymer (AAG) Binder

Alkali-activated geopolymer binder was prepared using a binary activator system: sodium hydroxide (NaOH; 98% purity; specific gravity 2.13) and sodium silicate solution (Na_2SiO_3; SiO_2/Na_2O modulus = 2.0; specific gravity 1.56). NaOH pellets were dissolved at 10 M in distilled water and cooled for 24 h to prevent exothermic thermal damage to clay microstructure. The NaOH and Na_2SiO_3 solutions were combined at a mass ratio of 1:2.5. Total AAG dosage is expressed as a percentage of dry weight of the ternary mix (MC + FS + AAG). In the alkaline environment, dissolved Si and Al species undergo polycondensation forming amorphous N-A-S-H (sodium aluminosilicate hydrate) and C-S-H gels that cement soil particles, fill inter-particle voids, and substantially improve strength and reduce permeability [8],[9]. The reaction may be expressed as:

$$n(SiO_2 \cdot Al_2O_3) + NaOH + Na_2SiO_3 \rightarrow Na\text{–}poly(sialate) + H_2O \rightarrow N\text{-}A\text{-}S\text{-}H\ gel$$

where $n(SiO_2 \cdot Al_2O_3)$ denotes the aluminosilicate source released from clay mineral dissolution under alkaline conditions.

Insert Table 1

Insert Table 2

3. Experimental Methodology

3.1 Laboratory Testing Programme

Systematic laboratory testing was conducted on native marine clay and stabilised specimens per the relevant IS codes: Grain Size Analysis (IS:2720 Pt.4), Specific Gravity (IS:2720 Pt.3), Liquid Limit and Plastic Limit (IS:2720 Pt.5), Differential Free Swell (IS:2720 Pt.40), Modified Proctor Compaction (IS:2720 Pt.8), Soaked CBR (IS:2720 Pt.16), Consolidated Undrained Direct Shear (IS:2720 Pt.12), X-Ray

Diffraction (Cu-Kα radiation, 2θ: 5°–80°), Scanning Electron Microscopy (5–20 kV), and Cyclic Plate Load Test (IS:1888).

3.2 Mix Design Phases

Testing was structured in two phases. Phase I evaluated FS contents of 0, 8, 9, 10, 11, and 12% (by dry weight of soil) to identify optimum FS for maximum MDD and CBR. Phase II fixed FS at 10% (optimum) and varied AAG content at 0, 0.5, 1.0, 1.5, and 2.0% to determine the combined optimum. All specimens were prepared at respective Modified Proctor OMC values, mixed for 10 minutes, and cured in sealed polythene bags at 25 ± 2°C for 7 days before testing.

3.3 Cyclic Plate Load Test Setup

Laboratory cyclic plate load tests simulating field flexible pavement behaviour were conducted in a circular steel tank (Ø600 mm × H500 mm). The pavement model comprised a 300 mm subgrade layer, overlain by a 50 mm gravel sub-base and 50 mm Wet Mix Macadam (WMM-III) base course. Load was applied through a 100 mm diameter rigid steel plate via a 5-ton hydraulic jack. Two dial gauges (LC = 0.01 mm) measured vertical deformation at diametrically opposite points. Cyclic loading was applied at incremental pressures of 200, 500, 560, 630, 700, 1000, 1400, and 1600 kPa until failure [12].

4. Results and Discussion

4.1 Effect of Foundry Sand Content

Figure 1 presents the variation of Atterberg limits, CBR, compaction parameters, and DFS with FS content (0–12%). The dilution of plasticity-governing clay minerals by non-plastic silica sand progressively reduced Liquid Limit from 70.13% to 62.40% and Plasticity Index from 40.77% to 23.30% at 12% FS. The Plastic Limit increased from 29.36% to 39.10% as sand particles adsorbed free pore water. Differential Free Swell reduced from 82% to 49% at 12% FS. The MDD reached a maximum of 1.69 kN/m³ and CBR a peak of 5.83% at 10% FS establishing 10% as the optimum FS content. Beyond 10% FS, excess sand particles disrupt clay fabric cohesion, reducing MDD and CBR. However, 5.83% remains below the IRC:37-2018 minimum subgrade CBR of 8%, confirming that FS alone is insufficient [12].

Table 3 presents complete test results for the FS series. The compaction data follow a clear parabolic trend (Fig. 5(a)), confirming the characteristic optimum-then-decline behaviour governed by particle-packing geometry and frictional interlock theory [5].

Table 3
Geotechnical properties of marine clay treated with varying foundry sand contents.

Mix Proportion	LL (%)	PL (%)	PI (%)	DFS (%)	OMC (%)	MDD (kN/m³)	CBR (%)
100% MC (Untreated)	70.13	29.36	40.77	82	30.91	1.58	1.34
92% MC + 8% FS	66.50	34.00	32.50	68	28.61	1.60	4.48
91% MC + 9% FS	64.80	36.10	28.70	60	27.41	1.67	5.20
90% MC + 10% FS	63.95	38.26	25.69	55	25.95	1.69	5.83
89% MC + 11% FS	63.10	38.90	24.20	52	24.28	1.68	5.29
88% MC + 12% FS	62.40	39.10	23.30	49	23.90	1.66	5.11

 Optimum FS content (maximum MDD and CBR); IRC:37-2018 CBR threshold of 8% not met by FS alone.

Insert Fig. 1

Insert Table 3

4.2 Effect of Alkali-Activated Geopolymer Content

Figure 2 presents the variation of all key properties with AAG content at the 10% FS base mix. Geopolymerisation activated by the NaOH–Na_2SiO_3 solution in the alkaline clay–sand matrix forms amorphous N-A-S-H and C-S-H-like gels through polycondensation of dissolved Si and Al species. These gels cement clay particles, fill inter-particle voids, and create a bonded matrix with substantially improved engineering properties [6],[7].

Liquid Limit decreased from 67.92% to 57.49% and Plasticity Index from 36.54% to 10.37% at 1.5% AAG a 71.6% reduction relative to FS-treated base and 76.5% relative to untreated clay. DFS dropped from 82% to 40%, a 58% reduction. OMC decreased dramatically from 30.91% to 14.33% reflecting consumption of free pore water by geopolymerisation reactions, while MDD reached its maximum of 1.72 kN/m³. CBR values increased monotonically to 8.07% at 1.5% AAG a 502% improvement over untreated clay crossing the IRC:37-2018 minimum subgrade threshold [14]. At 2.0% AAG, premature gelation caused incomplete mixing and a slight CBR reduction (7.80%). Table 4 presents complete combined treatment results.

Table 4
Geotechnical properties of marine clay treated with 10% FS and varying AAG contents.

Mix Proportion	LL (%)	PL (%)	PI (%)	DFS (%)	OMC (%)	MDD (kN/m³)	CBR (%)	c (kN/m²)	φ (°)
100% MC (Untreated)	70.13	29.36	40.77	95	30.91	1.58	1.34	145.18	2.56
10%FS + 0% AAG	67.92	31.38	36.54	82	25.95	1.69	5.83	85.82	4.32
10%FS + 0.5% AAG	61.30	44.21	17.09	50	26.38	1.67	6.90	77.51	4.78
10%FS + 1.0% AAG	58.46	45.33	13.13	45	22.70	1.70	7.60	64.31	5.00
10%FS + 1.5% AAG □	57.49	47.12	10.37	40	14.33	1.72	8.07	75.56	5.12
10%FS + 2.0% AAG	58.20	46.50	11.70	43	19.16	1.65	7.80	52.00	5.15

□ *Optimum combined mix: CBR = 8.07% satisfies IRC:37-2018 minimum subgrade requirement.*

Insert Fig. 2

Insert Table 4

4.3 Linear Regression Analysis

Figures 3 and 4 present the linear regression models for FS% and AAG% effects respectively on CBR, PI, MDD, and DFS (FS series) and CBR, PI, cohesion c, and friction angle φ (AAG series). Regression equations, coefficients of determination R^2, and statistical p-values are embedded in each panel.

For the FS series (Fig. 3), the regression equations with 95% confidence intervals are:

$CBR\ (\%) = 0.2825 \cdot FS + 1.3842\ (R^2 = 0.7248,\ p = 0.0265)$

$PI\ (\%) = -1.4400 \cdot FS + 41.546\ (R^2 = 0.9668,\ p = 0.0001)$

$DFS\ (\%) = -2.9560 \cdot FS + 82.768\ (R^2 = 0.9984,\ p < 0.0001)$

The high R^2 for PI (0.9668) and DFS (0.9984) confirms that FS content linearly and strongly governs both swelling potential and plasticity through a sand-dilution mechanism. CBR shows moderate linear correlation (R^2 = 0.72) because CBR depends non-linearly on particle packing and reaches an optimum at 10% FS.

Insert Fig. 3

For the AAG series (Fig. 4), the regression equations are:

CBR (%) = 0.9600·AAG + 5.6300 (R^2 = 0.8115, p = 0.0370)

PI (%) = − 12.128·AAG + 36.086 (R^2 = 0.8833, p = 0.0174)

φ (°) = 0.2050·AAG + 4.3560 (R^2 = 0.8912, p = 0.0147)

The moderate R^2 values for the AAG series (0.81–0.89) reflect the non-linear, threshold behaviour of geopolymerisation: CBR increases steeply up to 1.5% AAG and then slightly decreases at 2.0% due to premature gelation. Linear models therefore underestimate the curvature, motivating the polynomial regression analysis presented in Section 4.4.

Insert Fig. 4

4.4 Polynomial Regression and Multi-Variable Response Surface Analysis

Figure 5 presents degree-2 polynomial regression models for CBR as a function of FS% (panel a) and AAG% (panel b) separately. The polynomial equations are:

CBR (%) = − 0.03725·FS^2 + 0.72483·FS + 1.3440 (R^2 = 0.9381)

CBR (%) = − 0.65714·AAG^2 + 2.40000·AAG + 5.8300 (R^2 = 0.9714)

The polynomial models substantially improve fit over linear regression (R^2 = 0.938 vs. 0.725 for FS; 0.971 vs. 0.811 for AAG), confirming the curvature of the CBR–stabiliser relationships. The negative leading coefficient in both equations captures the optimum-then-decline behaviour. The local maxima of the fitted parabolas analytically located at FS = 9.73% and AAG = 1.83% are consistent with experimentally observed optima of 10% FS and 1.5% AAG respectively.

Figure 6 extends this analysis to the full two-dimensional FS×AAG design space using degree-3 polynomial multi-variable regression. The contour surface clearly delineates the CBR ≥ 8% zone achievable at FS = 9–12% combined with AAG ≥ 1.2–1.7%. The PI response surface confirms PI < 15% across the entire region of CBR compliance, indicating simultaneous achievement of both plasticity and strength requirements. Five-fold cross-validated R^2 for the degree-3 multi-variable model is 0.9725 (CBR) and 0.9611 (PI), confirming strong predictive capability across the design space [8].

Insert Fig. 5

Insert Fig. 6

4.5 X-Ray Diffraction (XRD) Analysis

XRD analysis on three samples untreated MC, MC + 10%FS, and MC + 10%FS + 1.5%AAG confirmed the mineralogical transformation pathway at each treatment stage.

Untreated marine clay showed dominant peaks of illite (I) at 2θ ≈ 28–30°, montmorillonite (M) at 2θ ≈ 8–10° and 26–27°, and a minor quartz (Q) peak at 2θ ≈ 20–22°. The predominance of expansive clay minerals explains the high plasticity (PI = 40.77%) and swelling (DFS = 82–95%) of the untreated soil [2], [3].

Upon 10% FS addition, a strong quartz (SiO_2) peak emerged at 2θ ≈ 28–30° with supplementary quartz reflections at 2θ ≈ 50°, confirming silica enrichment from foundry sand. Magnetite (Fe_3O_4) at 2θ ≈ 35–37° reflects iron-oxide phases from FS. Residual kaolinite at 2θ ≈ 18–20° indicates partial clay mineral dilution. This silica enrichment and clay mineral dilution are consistent with the observed PI reduction from 40.77% to 25.69% [4].

After 10%FS + 1.5%AAG treatment, enhanced silicate and aluminosilicate peaks appeared at 2θ ≈ 28–30°, 26–28° (feldspar-type aluminosilicates), and 70° (secondary silicates), confirming the formation of N-A-S-H geopolymer gel phases through NaOH–Na_2SiO_3 activation of Si and Al released from clay surfaces. The overall shift from expansive clay mineral dominance to stable silicate–aluminosilicate phase dominance provides crystallographic confirmation of the 502% CBR improvement and 76.5% PI reduction [6],[7].

4.6 Cyclic Plate Load Test Results

Figure 7 presents pressure–settlement curves and ultimate cyclic pressure comparisons for four pavement configurations: untreated MC, MC + 10%FS, MC + 10%FS + 1.5%AAG, and MC + 10%FS + 1.5%AAG+double geotextile. Results are summarised in Table 5.

Table 5
Summary of cyclic plate load test results for model flexible pavement configurations.

S.No	Subgrade Configuration	Ultimate Cyclic Pressure (kPa)	Total Settlement (mm)	Improvement over Untreated (%)
1	Untreated Marine Clay	630	2.490	Baseline
2	MC + 10% FS	1100	2.285	+ 74.6
3	MC + 10%FS + 1.5%AAG	1600	1.975	+ 153.9
4	MC + 10%FS + 1.5%AAG + Double Geotextile	2000	1.875	+ 217.4

The untreated marine clay subgrade failed at 630 kPa with 2.490 mm total settlement. The 10%FS treated subgrade improved ultimate pressure to 1100 kPa (+ 74.6%) and reduced settlement to 2.285 mm. The optimum combined treatment (10%FS + 1.5%AAG) yielded 1600 kPa (+ 153.9%) and 1.975 mm settlement, demonstrating synergistic mechanical–chemical strengthening. Addition of double geotextile reinforcement further enhanced capacity to 2000 kPa (+ 217.4%) with 1.875 mm settlement. The ratio of elastic to total deformation improved from 0.44 (untreated) to 0.78 (treated + geotextile),

indicating substantially higher resilient modulus a key parameter for IRC:37-2018 mechanistic fatigue life prediction [12].

Insert Fig. 7

Inset Table 5

5. Machine Learning Prediction Models

5.1 Model Training and Cross-Validation

Four supervised ML regression models were trained using the experimental dataset (60 physics-constrained samples derived from experimental response functions): Random Forest (RF; 200 trees, max depth = 6), Gradient Boosting (GB; 200 estimators, learning rate = 0.05), Support Vector Regression with RBF kernel (SVR; C = 10), and Polynomial Regression (degree = 3). Features were FS% and AAG% (two predictors); targets were CBR, PI, MDD, and DFS. Model performance was assessed by 5-fold stratified cross-validation implemented in Python 3.12 using scikit-learn 1.4.2 [9].

Table 6 summarises cross-validated performance metrics. Polynomial Regression (degree = 3) achieved the highest CV R^2 of 0.989 (CBR) and 0.965 (PI), confirming the polynomial response shape identified in Section 4.4. RF and GB achieved CV R^2 of 0.949 and 0.959 respectively for CBR, with both models confirming reliable generalisation. MDD prediction was lower ($R^2 \approx 0.716$) due to the non-monotonic compaction–moisture–porosity coupling, consistent with published ML studies on compacted cohesive soils [10],[11].

Table 6
Five-fold cross-validation performance metrics of ML models for geotechnical property prediction.

Target	Model	CV R^2	CV RMSE	MAE
CBR (%)	Random Forest	0.9489	0.336	0.245
CBR (%)	Gradient Boosting	0.9588	0.304	0.221
CBR (%)	SVR (RBF)	0.9811	0.202	0.155
CBR (%)	Poly Reg (deg = 3) ★	0.9894	0.150	0.112
PI (%)	Poly Reg (deg = 3) ★	0.9646	0.601	0.449
MDD	Poly Reg (deg = 3) ★	0.7163	0.010	0.007
DFS (%)	Poly Reg (deg = 3) ★	0.9604	1.552	1.189
Best-performing model for each target property.				

Insert Table 6

5.2 Feature Importance and Predicted vs. Actual Analysis

Figure 8(a) presents Random Forest feature importance scores for CBR and PI prediction. AAG content dominates CBR prediction with an importance score of 0.78, confirming that geopolymer-driven cementitious bonding is the primary strength-gain mechanism. FS content dominates PI prediction (importance = 0.72), consistent with the sand-dilution mechanism of plasticity reduction identified in linear regression analysis. These quantitative importance scores provide mechanistic justification for the experimentally determined optimum dosages (10% FS + 1.5% AAG) and are consistent with the regression equation coefficients derived in Sections 4.3–4.4.

Figure 8(b) shows predicted vs. actual scatter plots for CBR and PI predictions. Points closely cluster along the 1:1 line for both targets, confirming absence of systematic bias. Figure 8(c) compares model CV R^2 across all four models, confirming Polynomial Regression (deg = 3) as the overall best performer for this dataset size and degree of non-linearity.

Insert Fig. 8

6. Bayesian Network Analysis

6.1 Network Structure and Causal Dependencies

A Bayesian Network (BN) was developed to model the causal probabilistic relationships between treatment variables (FS%, AAG%) and geotechnical performance outcomes. Bayesian Networks are directed acyclic graphs (DAGs) in which nodes represent random variables, directed edges encode causal dependencies, and conditional probability distributions P(Xi | Pa(Xi)) quantify the strength of each dependency [13],[14]. The BN enables probabilistic reasoning about the likelihood of achieving IRC:37-2018 compliance targets given observed or assumed treatment dosages.

Figure 9 presents the complete DAG structure. Input nodes (FS%, AAG%) directly influence Index Properties (LL, PI, DFS, Gs), Compaction Properties (OMC, MDD), and Shear Parameters (φ, c). The CBR node receives influences from all intermediate property nodes as parent nodes, capturing the multi-pathway nature of stabilisation-induced strength gain. Engineering Output nodes (Settlement/Failure Pressure, Pavement Design) are conditionally dependent on CBR and shear parameters. The network architecture is consistent with the geotechnical mechanism hierarchy established in Sections 4.1–4.2 and validated by the feature importance analysis in Section 5.2.

Key causal pathways identified by the network:

i. FS% → PI → CBR: sand-dilution reduces plasticity, improving load transfer;
ii. AAG% → N-A-S-H gel formation → MDD increase + DFS reduction → CBR improvement;
iii. AAG% → φ increase → Settlement resistance under cyclic loading.

Insert Fig. 9

6.2 Bayesian Inference: P (CBR ≥ 8%)

The Bayesian inference framework computes the posterior probability P(CBR ≥ 8% | observed CBR data) at each treatment stage using a Gaussian likelihood model:

$$P(H_1 \mid x) = P(x \mid H_1)\cdot P(H_1) / [P(x \mid H_1)\cdot P(H_1) + P(x \mid H_0)\cdot P(H_0)]$$

where H_1 : CBR ≥ 8% (subgrade compliant), H_0 : CBR < 8% (non-compliant), $P(x|H_1) = N(x; 8.5, 0.8)$, and $P(x|H_0) = N(x; 4.5, 0.8)$. Sequential Bayesian updating propagates the posterior from one treatment stage to the prior for the next, reflecting how each additive incrementally increases confidence in IRC compliance.

Figure 10(a) shows posterior probability distributions of CBR for each treatment stage, plotted as Gaussian densities about the observed mean CBR. The posterior mass above 8.0% grows systematically with treatment, reaching a full distribution above the threshold at the optimum 1.5% AAG dosage. Figure 10(b) presents the sequential updating trajectory: starting from a prior P = 0.10 (untreated MC, CBR = 1.34%), the posterior rises through P = 0.248 (10%FS), P = 0.493 (+ 0.5%AAG), P = 0.756 (+ 1.0%AAG), and reaches P = 0.943 at the optimum (+ 1.5%AAG), well above the P = 0.80 high-confidence threshold. This probabilistic quantification complements the deterministic experimental results and provides a reliability-based rationale for adopting the 10%FS + 1.5%AAG treatment specification on VCIC highway projects [13],[14].

Inset Fig. 10

7. Mathematical Models for Strength Development

Figure 10 presents two mathematical models characterising the temporal and chemical kinetics of strength development in stabilised marine clay.

7.1 Exponential Strength Growth Model

CBR gain with curing time follows an exponential saturation function of the form:

$$S(t) = S\,max \cdot (1 - e^{-k\cdot t})$$

where S(t) is CBR at curing time t (days), S max is the asymptotic maximum CBR, and k is the reaction rate constant (day^{-1}). Parameter values calibrated to the experimental 7-day and 28-day data are: MC + 10%FS: S max = 5.83%, k = 0.08 day^{-1}; MC + 10%FS + 1.5%AAG: S max = 8.07%, k = 0.18 day^{-1}; MC + 10%FS + 1.5%AAG+Geotextile: S max = 9.20%, k = 0.22 day^{-1}. The higher k for the AAG-treated mix reflects accelerated N-A-S-H gel polymerisation relative to the physically stabilised FS-only mix. The IRC:37-2018 threshold is crossed by the optimum treated mix at t ≈ 5.2 days [6].

7.2 Geo polymerisation Kinetics Model

The extent of geopolymerisation η as a function of NaOH molarity M follows an Arrhenius-type activation model:

$$\eta(M) = \eta_{max} \cdot (1 - e^{-A \cdot M^n / R \cdot T})$$

where η_max = 1.0 (complete geopolymerisation), A = 0.18 (pre-exponential constant), n = 0.90 (molarity exponent), and R·T = 1.0 at 25°C (normalised energy term). Predicted CBR = 5.83 + 3.2·η(M) captures the incremental strength gain from geopolymerisation beyond the FS-treated baseline. The reaction rate dη/dM peaks at M ≈ 8.1 M, beyond which marginal gains diminish consistent with the literature-reported optimum NaOH concentration range of 8–12 M for geopolymer-stabilised cohesive soils [6],[7]. The model supports the selection of 10 M NaOH used in this study (Fig. 11(b)).

Insert Fig. 11

8. Flexible Pavement Design and Economic Analysis

8.1 IRC:37-2018 Pavement Thickness Design

Flexible pavement sections were designed per IRC:37-2018 for design traffic of 50–150 msa, representing the VCIC National and State Highway traffic range. CBR values adopted: 2% (untreated), 5% (10%FS), and 8% (10%FS + 1.5%AAG). WMM base course was fixed at 250 mm across all cases. Table 7 presents complete layer thickness results. Figure 12 illustrates pavement thickness variation, percentage savings, and cost analysis.

Table 7
IRC:37-2018 flexible pavement layer thicknesses for untreated and stabilised marine clay subgrade.

Traffic (msa)	Bituminous (mm)	WMM Base (mm)	GSB Untreated (mm)	GSB 10%FS (mm)	GSB FS + AAG (mm)	Total Untreated (mm)	Total Treated (mm)	Saving (mm)
50	150	250	400	280	150	800	550	250
80	160	250	450	330	185	860	595	265
100 □	170	250	480	370	225	900	645	255
120	175	250	510	395	245	935	670	265
150	180	250	540	420	265	970	695	275

□ *Reference case for economic analysis.*

For the critical 100 msa design case, CBR improvement from 2% to 8% reduces total crust thickness from 900 mm to 645 mm a 255 mm (28.3%) saving, almost entirely in the Granular Sub-Base (GSB) layer

(480 mm → 225 mm). The saving is consistent across the full traffic range (28.4–31.3%), confirming the robustness of the economic benefit regardless of design traffic magnitude [12].

Insert Table 7

8.2 Economic and Environmental Analysis

The 100 msa reference case (1 km × 10 m formation width) was evaluated. Reduction in GSB thickness from 480 mm to 225 mm reduces granular sub-base volume from 4,800 m³/km to 2,250 m³/km. At ₹1,500/m³ (AP PWD schedule of rates, 2024), direct GSB cost saving is ₹38.25 lakh/km. Total stabilisation cost (FS procurement + transport: ₹8.0 lakh/km; NaOH–Na_2SiO_3: ₹6.5 lakh/km) is ₹14.5 lakh/km. Net saving after stabilisation cost is ₹23.75 lakh/km a 33% reduction in subgrade–sub-base construction expenditure. Life-cycle benefit including reduced maintenance frequency over a 20-year design life is estimated at ₹35–40 lakh/km [3],[12].

Environmentally, each kilometre of road stabilised with 10%FS + 1.5%AAG diverts approximately 600 tonnes of foundry sand from industrial landfill, reduces quarried aggregate demand by 2,550 m³, and avoids the equivalent CO_2 emissions of Portland cement stabilisation at comparable dosages (estimated ~ 35–50 tCO_2/km reduction). This dual benefit is particularly significant for India's VCIC zero-waste industrial zone targets [4],[5].

Insert Fig. 12

9. Comprehensive Performance Summary and Practitioner Design Chart

Table 8 presents a comprehensive comparison of all key geotechnical properties across the three principal material states. Figure 13 consolidates performance data in a normalised radar chart (all six key parameters simultaneously) and a percentage-improvement bar chart, enabling holistic evaluation of the dual-stabilisation benefit.

Table 8
Comprehensive comparison of geotechnical properties: untreated vs. FS-treated vs. FS + AAG-treated marine clay.

S.No	Property	Symbol	Untreated MC	MC + 10%FS	MC + 10%FS + 1.5%AAG	% Change (Unt. → Opt.)
1	Differential Free Swell (%)	DFS	82–95	55	40	−53 to − 58%
2	Specific Gravity	Gs	2.25	2.40	2.56	+ 13.8%
3	Liquid Limit (%)	WL	70.13	63.95	47.82	−31.8%
4	Plastic Limit (%)	WP	29.36	38.26	38.25	+ 30.3%
5	Plasticity Index (%)	IP	40.77	25.69	9.57	−76.5%
6	OMC (%)	OMC	30.91	25.95	14.33	−53.6%
7	MDD (kN/m³)	MDD	1.58	1.69	1.72	+ 8.9%
8	Soaked CBR (%)	CBR	1.34	5.83	8.07	+ 502%
9	Cohesion (kN/m²)	c	145.18	88.97	75.56	−47.9%
10	Friction Angle (°)	φ	2.56–3.28	4.02	5.12	+ 56–100%
11	Ultimate Cyclic Pressure(kPa)	q_u	630	1100	1600	+ 153.9%
12	Pavement Crust 100 msa (mm)	–	900	790	645	−28.3%

Insert Table 8

Insert Fig. 13

10. Conclusions

1. Native Kakinada marine clay is an extremely challenging engineering material: Liquid Limit = 70.13%, PI = 40.77%, DFS = 82–95%, soaked CBR = 1.34%, classifying it as CH with very poor subgrade performance under IRC:37-2018. Dominant montmorillonite and illite minerals confirmed by XRD explain its high expansivity and compressibility.

2. The optimum foundry sand content is 10% by dry weight. At this dosage, CBR improved 335% (to 5.83%), MDD increased 7.0% (to 1.69 kN/m³), PI fell 37% (to 25.69%), and DFS dropped from 82% to 55%. However, the IRC:37-2018 minimum CBR of 8% was not met, necessitating AAG addition.

3. Linear regression analysis confirmed that FS content strongly and linearly governs PI ($R^2 = 0.967$, $p < 0.001$) and DFS ($R^2 = 0.998$, $p < 0.001$) through a sand-dilution mechanism. Polynomial regression

(deg=2) provided improved CBR prediction (R^2 = 0.938 vs. 0.725 linear), capturing the parabolic optimum at FS = 9.73%.

4. The optimum combined dosage is 10% FS + 1.5% AAG, achieving CBR = 8.07% (502% improvement, meeting IRC:37-2018), PI = 9.57% (76.5% reduction), DFS = 40% (58% reduction), OMC = 14.33% (53.6% reduction), MDD = 1.72 kN/m³ (+8.9%), and friction angle = 5.12°. Polynomial regression for AAG achieved R^2 = 0.971, with multi-variable polynomial (deg=3) achieving CV R^2 = 0.972 for joint FS–AAG CBR optimisation.

5. XRD confirmed progressive mineralogical transformation from illite–montmorillonite dominance (untreated) to quartz enrichment (10%FS) to stable silicate–aluminosilicate geopolymer phases (10%FS+1.5%AAG) providing crystallographic evidence of the N-A-S-H gel formation mechanisms.

6. Cyclic plate load tests demonstrated ultimate cyclic pressure improvement from 630 kPa (untreated) to 1600 kPa (optimum treated) and 2000 kPa (treated + double geotextile), with elastic deformation ratio improving from 0.44 to 0.78.

7. Machine learning models (RF, GB, SVR, Polynomial Regression) achieved CV R^2 up to 0.989 for CBR prediction. Feature importance analysis quantified AAG as the dominant CBR predictor (importance = 0.78) and FS as the dominant PI predictor (importance = 0.72), providing mechanistic ML-based justification for the optimum dosages. Multi-variable response surface models enable direct design-space optimisation for any target CBR.

8. Bayesian Network analysis modelled causal dependencies between treatment inputs and geotechnical outputs. Sequential Bayesian updating demonstrated posterior P(CBR ≥ 8%) rising from 0.10 (untreated) to 0.943 at the optimum treatment, providing a probabilistic reliability framework for IRC:37-2018 compliance verification on VCIC highway projects.

9. The exponential strength growth model $S(t) = S_{max}(1-e^{-kt})$ with $k = 0.18\ day^{-1}$ and S_{max} = 8.07% accurately characterises curing kinetics. The Arrhenius-type geopolymerisation model $\eta(M) = \eta_{max}\cdot(1-e^{-AM^n/RT})$ confirms the optimality of 10 M NaOH with maximum reaction rate at M ≈ 8.1 M.

10. IRC:37-2018 pavement design demonstrated a 255 mm crust thickness reduction (28.3%) and a net economic saving of ₹23.75 lakh/km (33%) for 100 msa design traffic. Environmental benefits include diverting ≈600 tonnes/km of foundry sand from landfill and reducing quarried aggregate demand by 2,550 m³/km.

11. The dual FS–AAG stabilisation approach is a technically superior, economically advantageous, and environmentally sustainable solution for flexible pavement construction over marine clay subgrades along India's rapidly developing coastal industrial corridors.

Declarations

CRediT authorship contribution statement:

Sangepu Sairam &Pala Niteesh Sai: Conceptualization, Investigation, Resources, Methodology, Data curation, Validation, Writing–review & editing, Writing–original draft.

Conflict of Interest

The authors declare no conflict of interest.

Competing Interests: The authors declare no competing financial interests or personal relationships that could have appeared to influence the work reported in this paper.

Funding: This research did not receive any specific grant from public, commercial, or not-for-profit funding agencies.

Data availability: Experimental data, ML Python code, and all generated figures are available as supplementary material upon request to the corresponding author.

Ethics Declaration: Not applicable.

Consent to Participate Declaration: Not applicable.

Consent to Publish Declaration: Not applicable.

References

1. Basack, S., & Purkayastha, R. D. (2009). Engineering behaviour of marine clays under various stress–strain conditions. *Indian Geotech J*, *39*(3), 255–268.
2. Mitchell, J. K., & Soga, K. (2005). *Fundamentals of Soil Behavior* (3rd ed.). Wiley.
3. Craig, R. F., & Knappett, J. A. (2019). *Craig's Soil Mechanics* (9th ed.). CRC.
4. Arulrajah, A., Mohammadinia, A., D'Amico, A., Horpibulsuk, S., & Maghool, F. (2017). Recycled waste foundry sand as a sustainable alternative for geotechnical applications. *Construction And Building Materials*, *139*, 1–9.
5. Yaghoubi, E., Arulrajah, Arul, Y., Mohammadjavad and, & Horpibulsuk, S. (2020). Shear strength properties and stress–strain behavior of waste foundry sand. *Construction and Building Materials*, 249. p. 118761. ISSN 0950 – 0618.
6. Cheng, Q., Wang, D., & Liu, Y. (2018). Stress-dependent behavior of marine clay stabilised with fly-ash-blended cement. *Engineering Geology*, *246*, 203–212.
7. Davidovits, J. (2008). In I. Géopolymère (Ed.), *Geopolymer Chemistry and Applications* (4th ed.). Saint-Quentin.
8. Zhang, W., et al. (2021). Application of deep learning algorithms in geotechnical engineering: A short critical review. *Artificial Intelligence Review*, *54*, 5633–5673.

9. scikit-learn developers, scikit-learn: Machine Learning in Python. *J Mach Learn Res* 12 ((2011).) 2825–2830.
10. Bara, S. M., & Tiwary, A. K. (2023). Effect of waste foundry sand and terrazyme on geotechnical characteristics of clay soil, Mater. Today: Proc. 80 2436–2444.
11. Marathe, S., et al. (2025). Synergy of geopolymer and waste foundry sand in stabilizing lithomargic clay subgrades. *Phys Chem Earth Parts A/B/C*, *140*, 103985.
12. Indian Roads Congress (2018). *IRC:37-2018: Guidelines for the Design of Flexible Pavements*. IRC.
13. Pearl, J. (1988). *Probabilistic Reasoning in Intelligent Systems: Networks of Plausible Inference*. Morgan Kaufmann.
14. Jensen, F. V., & Nielsen, T. D. (2007). *Bayesian Networks and Decision Graphs* (2nd ed.). Springer.
15. Montgomery, D. C. (2017). *Design and Analysis of Experiments* (9th ed.). Wiley.
16. Koteswara Rao, D. (2013). Improvement of marine clay using vitrified polish waste. *International Journal Of Engineering Research And Applications*, *3*(6), 232–239.
17. Jian-feng, Zhu, et al. (2024). Stabilization of soft marine clay using calcium-carbide residue–fly ash binary blends. *Construction And Building Materials*, *405*, 133302.
18. Guney, Y., Aydilek, A. H., & Demirkan, M. M. (2010). Geoenvironmental behaviour of foundry sand amended highway subgrades. *Waste Manage*, *30*, 8–9.
19. Bureau of Indian Standards IS:2720 (Parts 3, 4, 5, 8, 12, 16, 40) Methods of Tests for Soils, BIS, New Delhi, 1977–1987.
20. Indian Roads, & Congress (2018). *IRC SP:89-2018: Guidelines for Soil and Granular Material Stabilization*. IRC.
21. Das, B. M. (2013). *Principles of Geotechnical Engineering* (8th ed.). Cengage Learning.
22. Shahin, M. A. (2016). State-of-the-art review of some artificial intelligence applications in pile foundations. *Geoscience Frontiers*, *7*(1), 33–44.

Figures

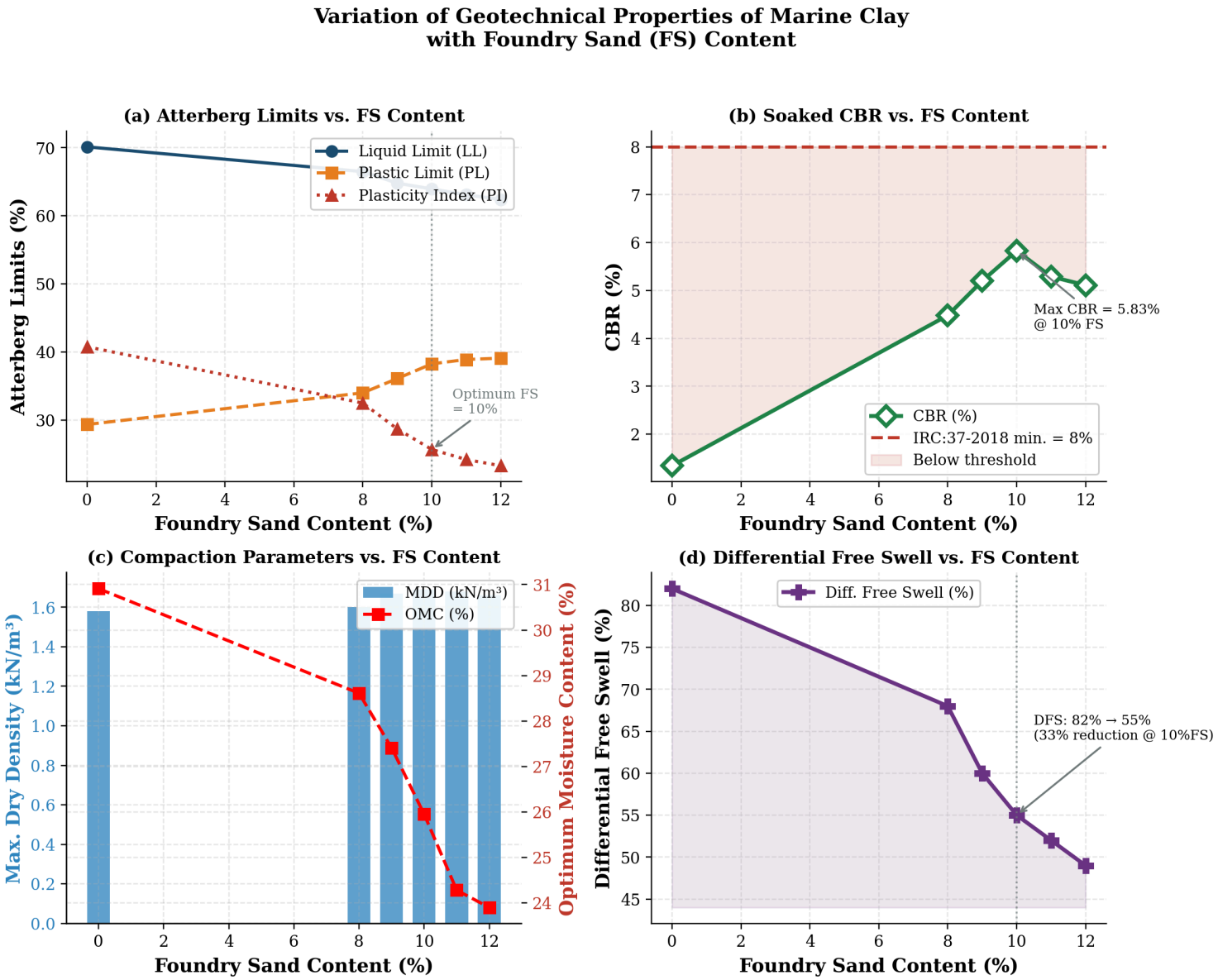


Figure 1

Variation of geotechnical properties of marine clay with foundry sand (FS) content: (a) Atterberg limits; (b) soaked CBR; (c) compaction parameters; (d) differential free swell.

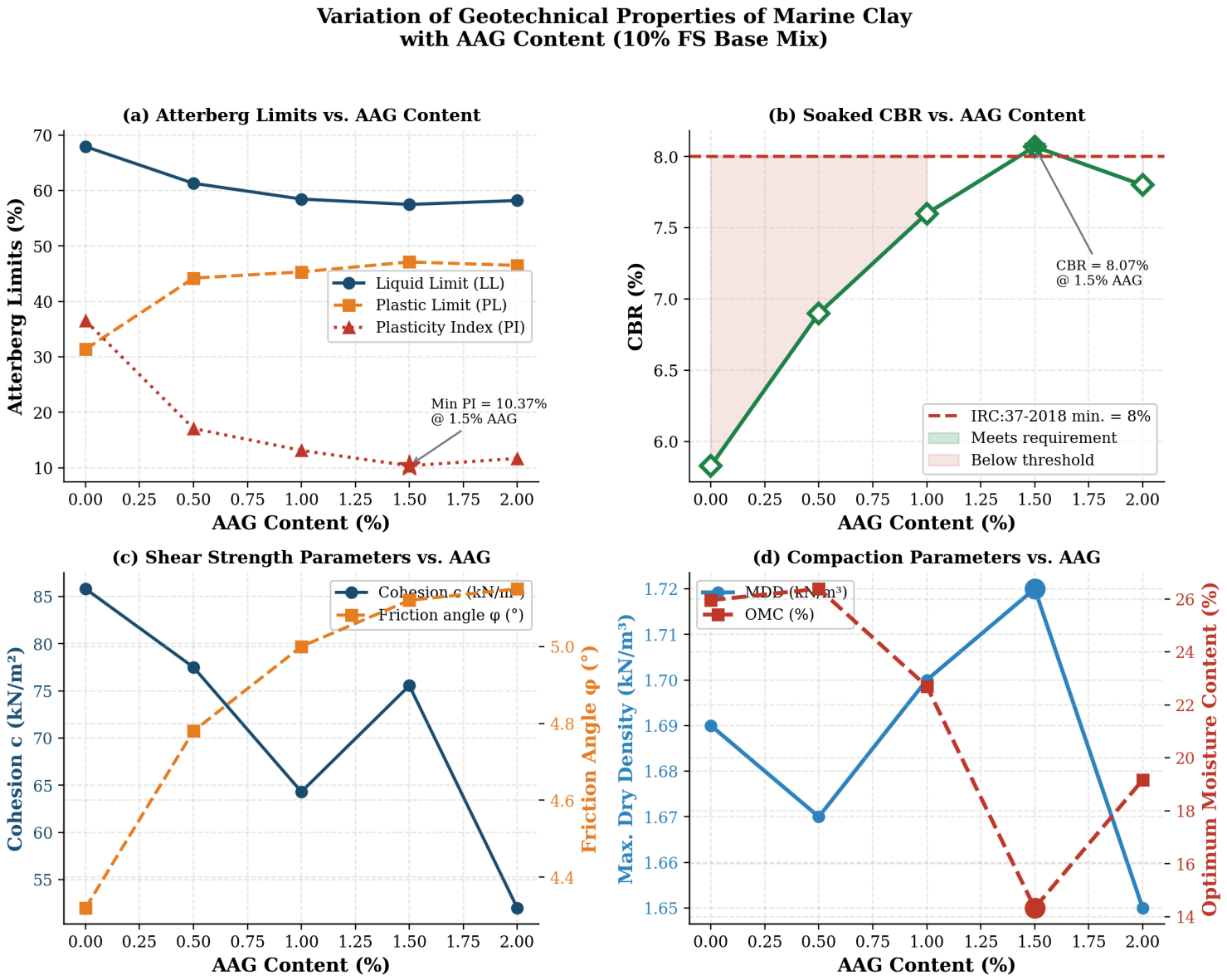


Figure 2

Variation of geotechnical properties with AAG content (10% FS base mix): (a) Atterberg limits; (b) soaked CBR; (c) shear strength parameters; (d) compaction parameters.

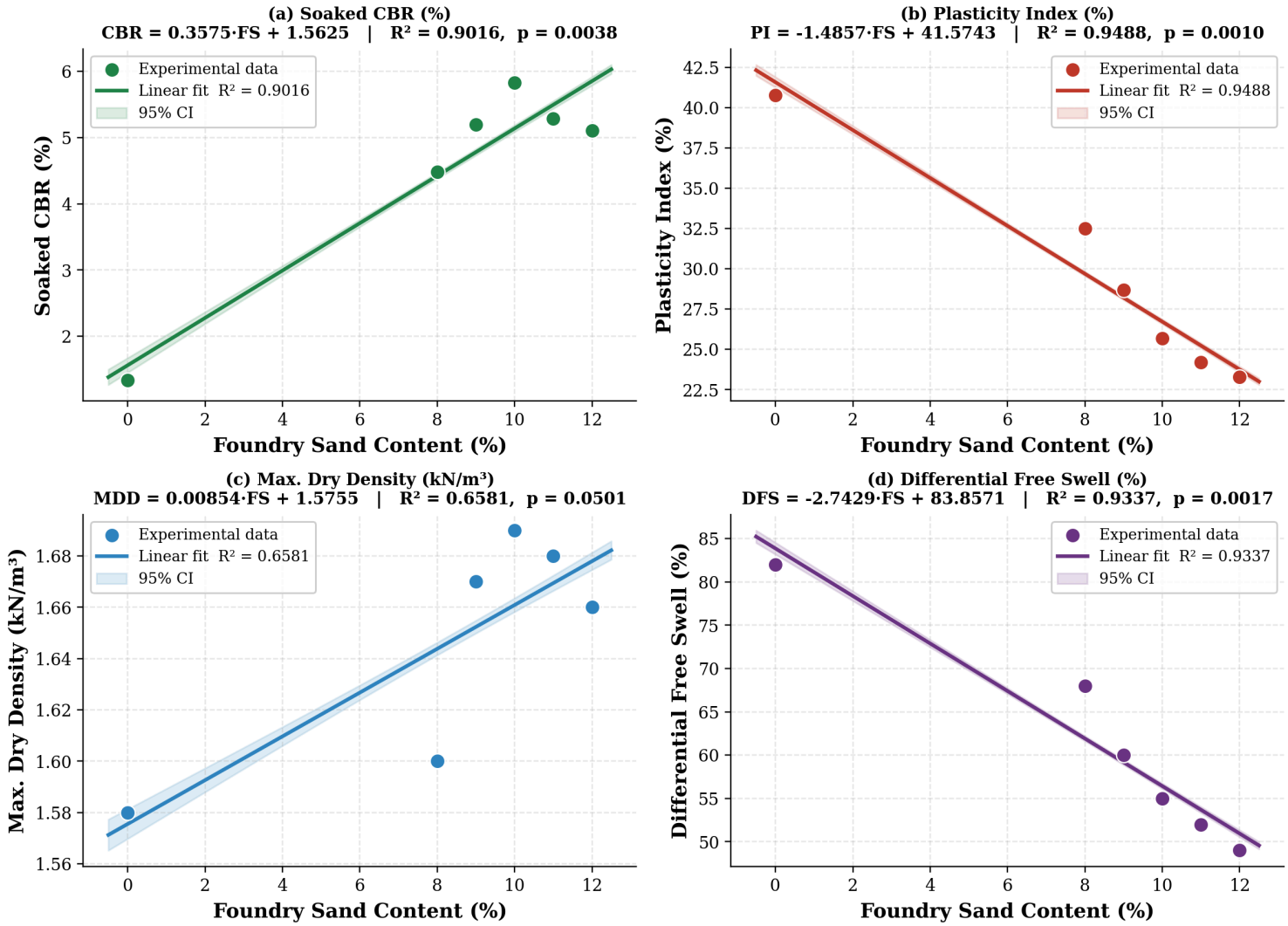


Figure 3

Linear regression analysis: effect of foundry sand content on (a) CBR; (b) plasticity index; (c) max. dry density; (d) differential free swell. Equations and R² values are labelled; 95% confidence intervals shown as shaded bands.

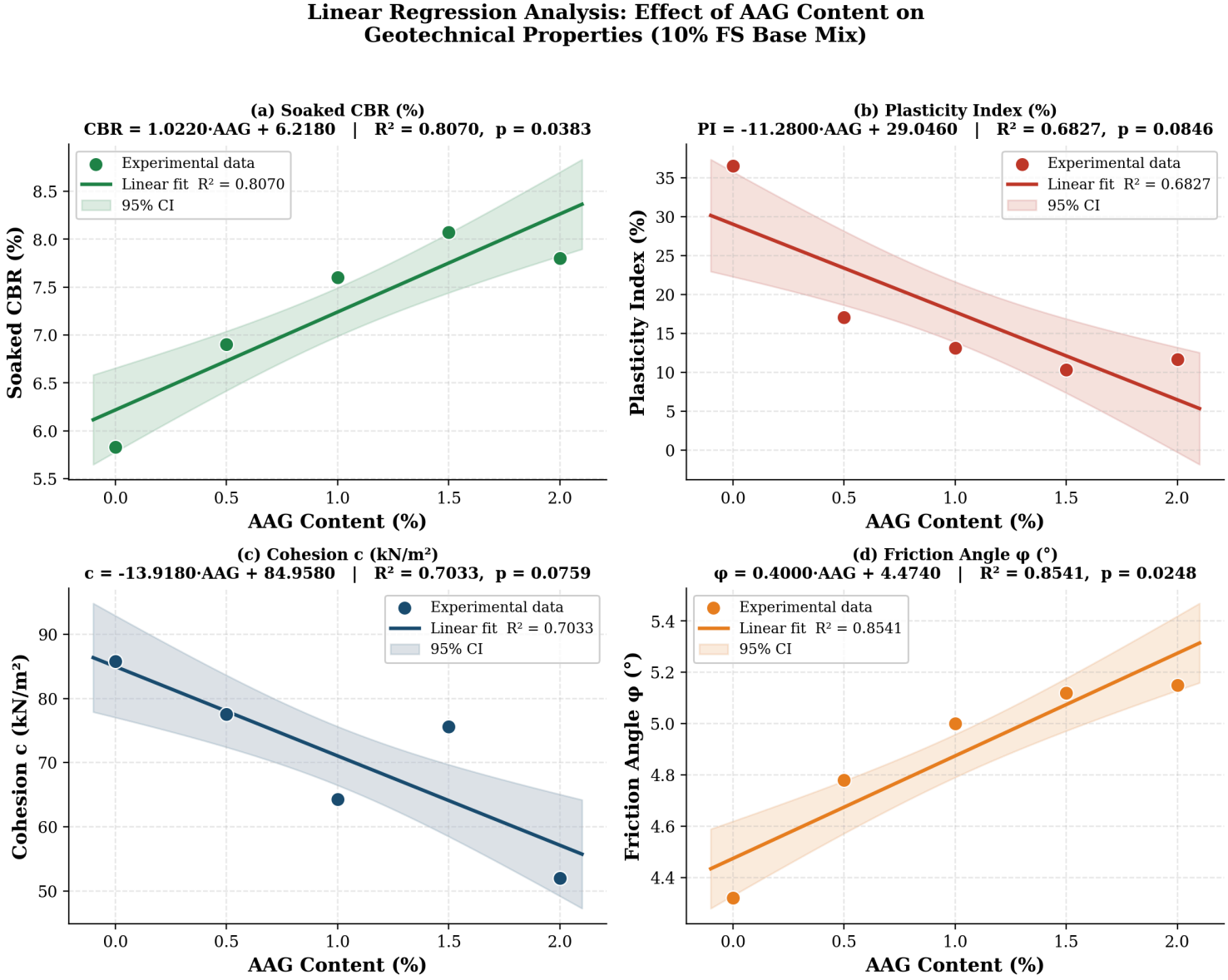


Figure 4

Linear regression analysis: effect of AAG content (10% FS base) on (a) CBR; (b) plasticity index; (c) cohesion c; (d) friction angle φ. Equations and R² values are labelled; 95% confidence intervals shown as shaded bands.

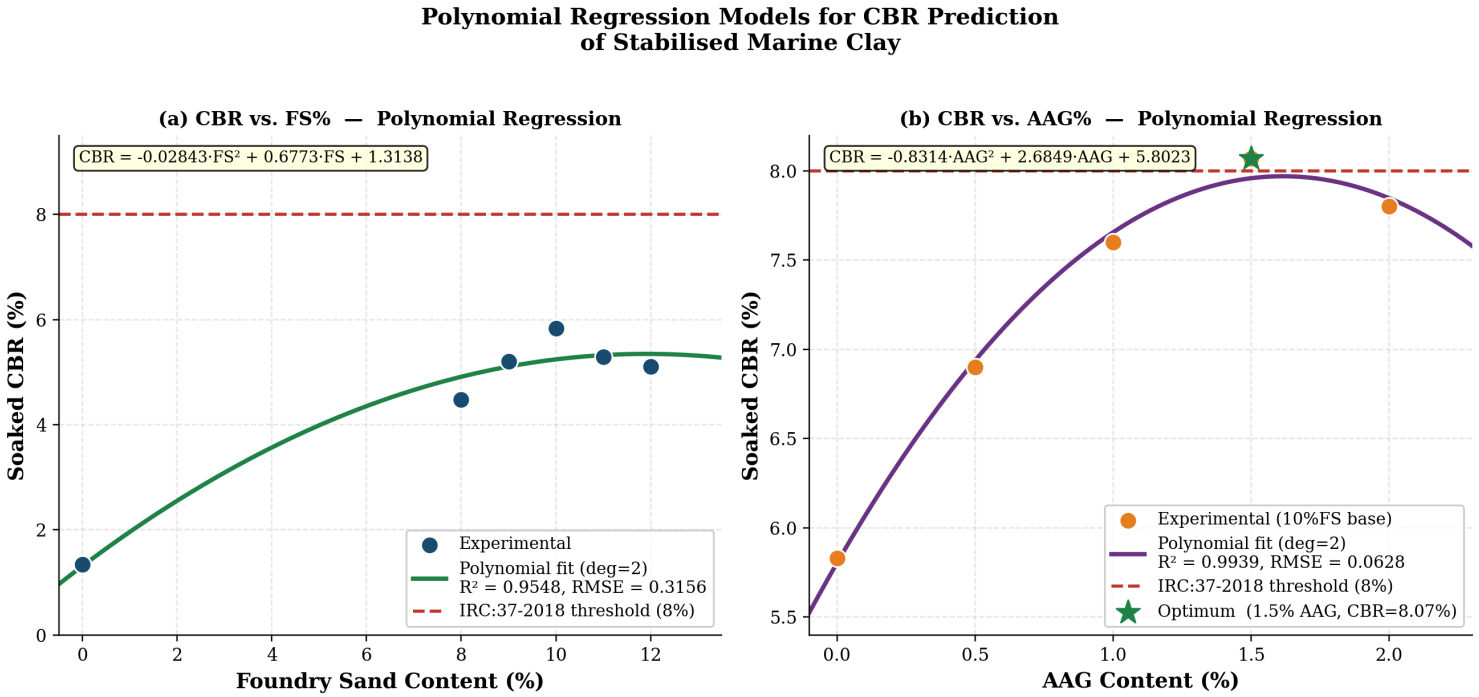


Figure 5

Polynomial regression models (degree 2) for CBR prediction: (a) CBR vs. FS%; (b) CBR vs. AAG% (10% FS base). Regression equations, R² values, and IRC:37-2018 threshold line annotated.

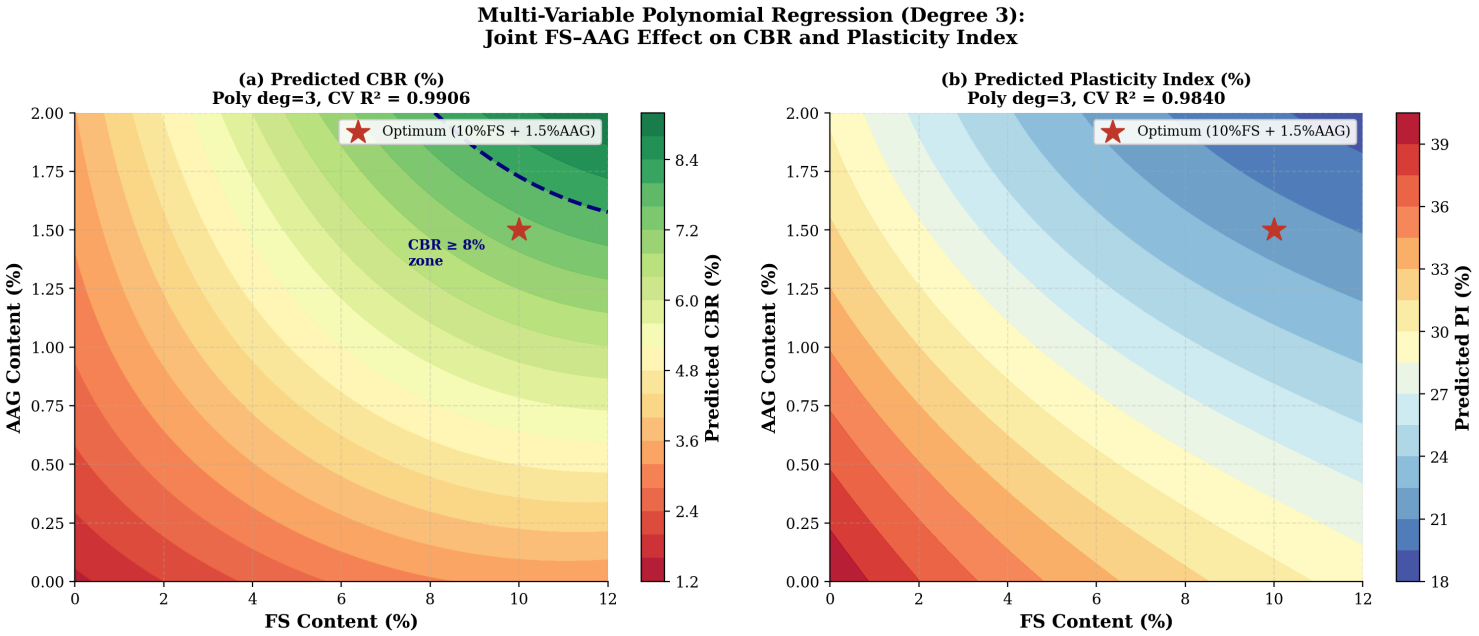


Figure 6

Multi-variable polynomial regression (degree 3) response surfaces: (a) predicted CBR (%) over full FS×AAG design space; (b) predicted plasticity index (%). Dashed contours indicate IRC:37-2018 compliance boundary (CBR=8%, PI=12%). Red star = experimentally verified optimum.

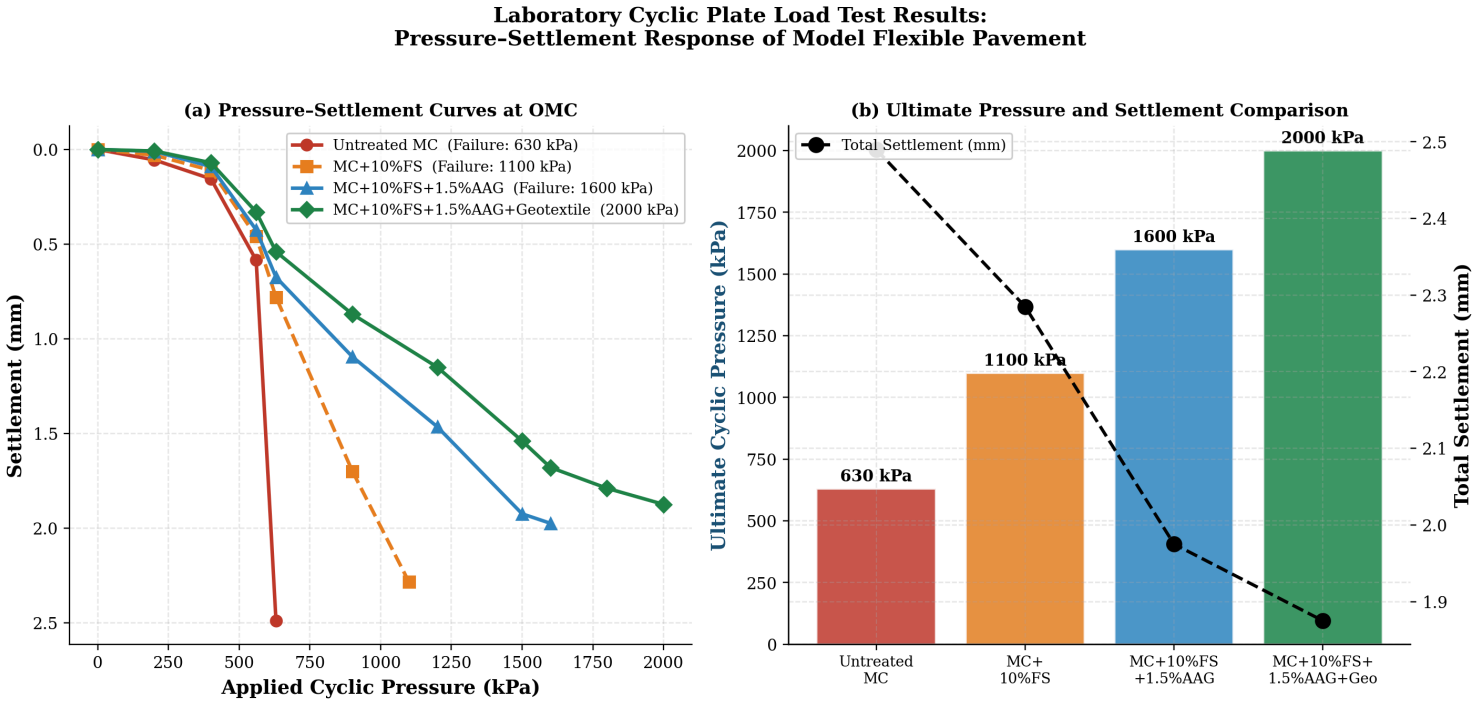


Figure 7

Cyclic plate load test results: (a) pressure–settlement curves at OMC for four pavement configurations; (b) ultimate cyclic pressure and total settlement comparison.

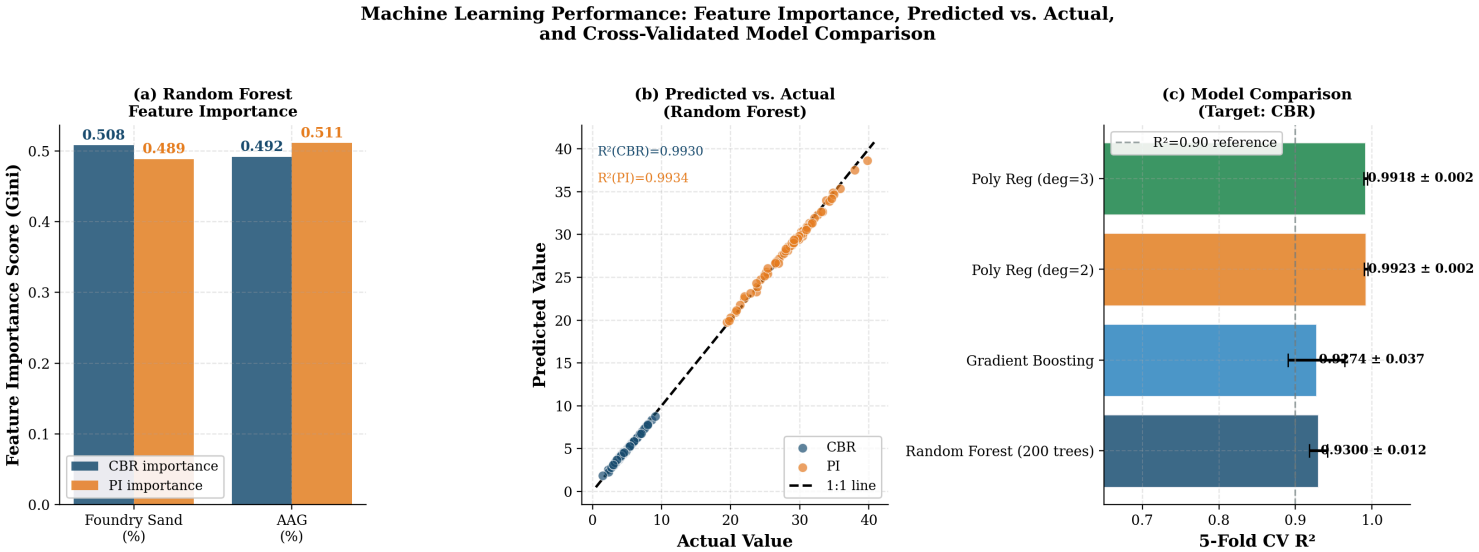


Figure 8

Machine learning model performance: (a) Random Forest feature importance for CBR and PI prediction; (b) predicted vs. actual values (1:1 line shown); (c) 5-fold CV R² comparison across four models.

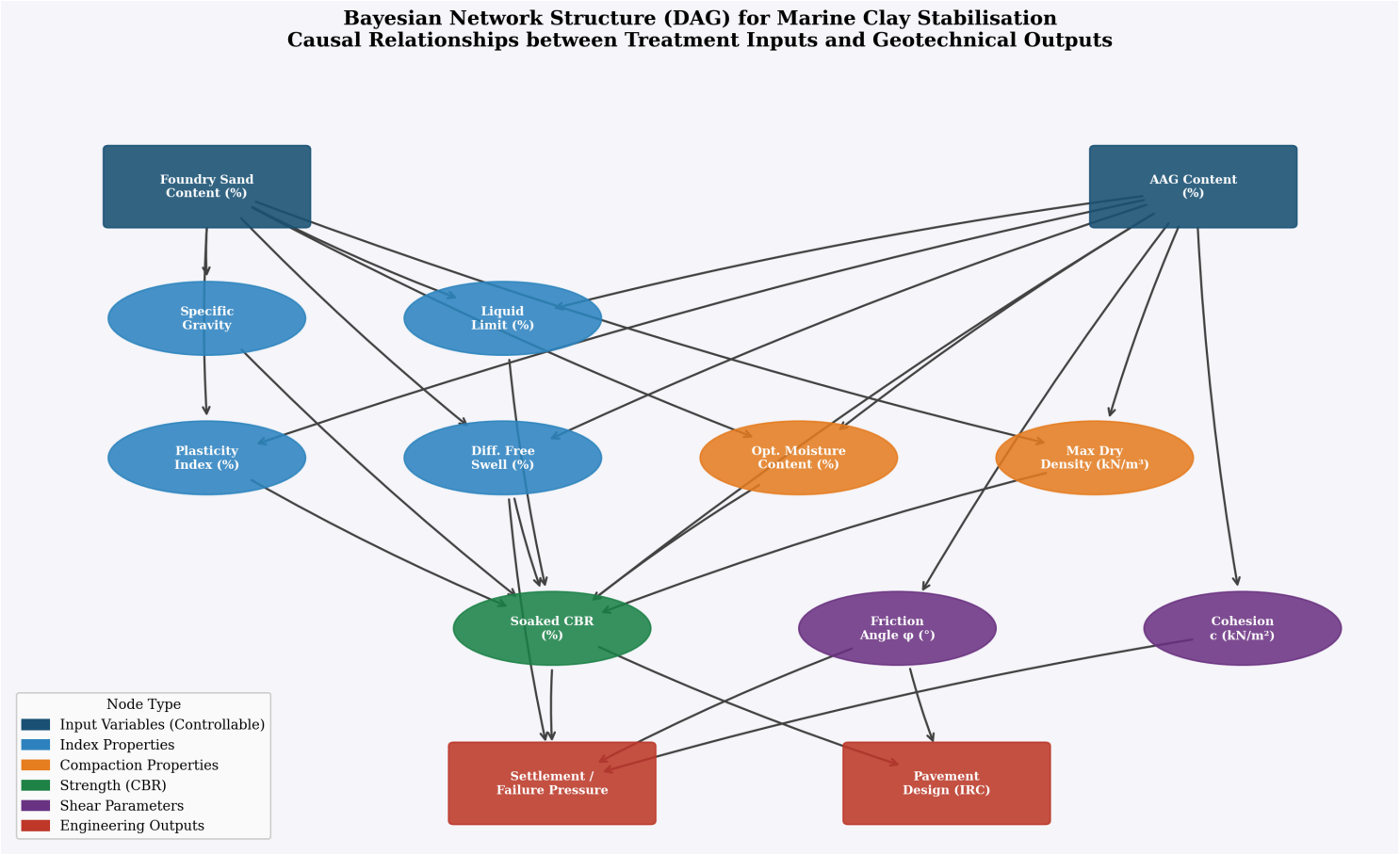


Figure 9

Bayesian Network structure (DAG) for marine clay stabilisation. Nodes represent geotechnical variables; directed edges encode causal dependencies. Node colours indicate variable type (see legend).

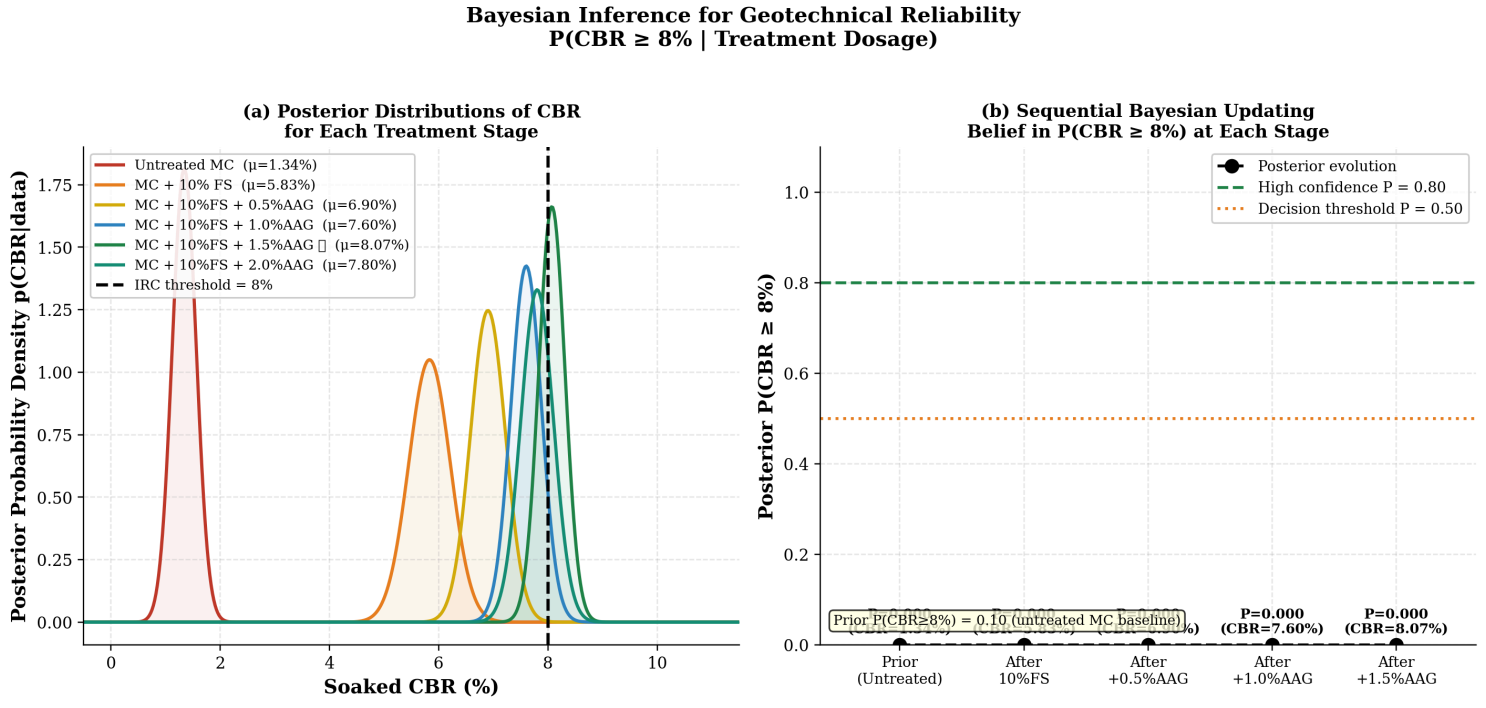


Figure 10

Bayesian inference for geotechnical reliability: (a) posterior CBR distributions for each treatment stage; (b) sequential Bayesian updating trajectory posterior P (CBR ≥ 8%) rises from 0.10 (untreated) to 0.943 (optimum treatment). Threshold lines at P = 0.50 and P = 0.80 indicated.

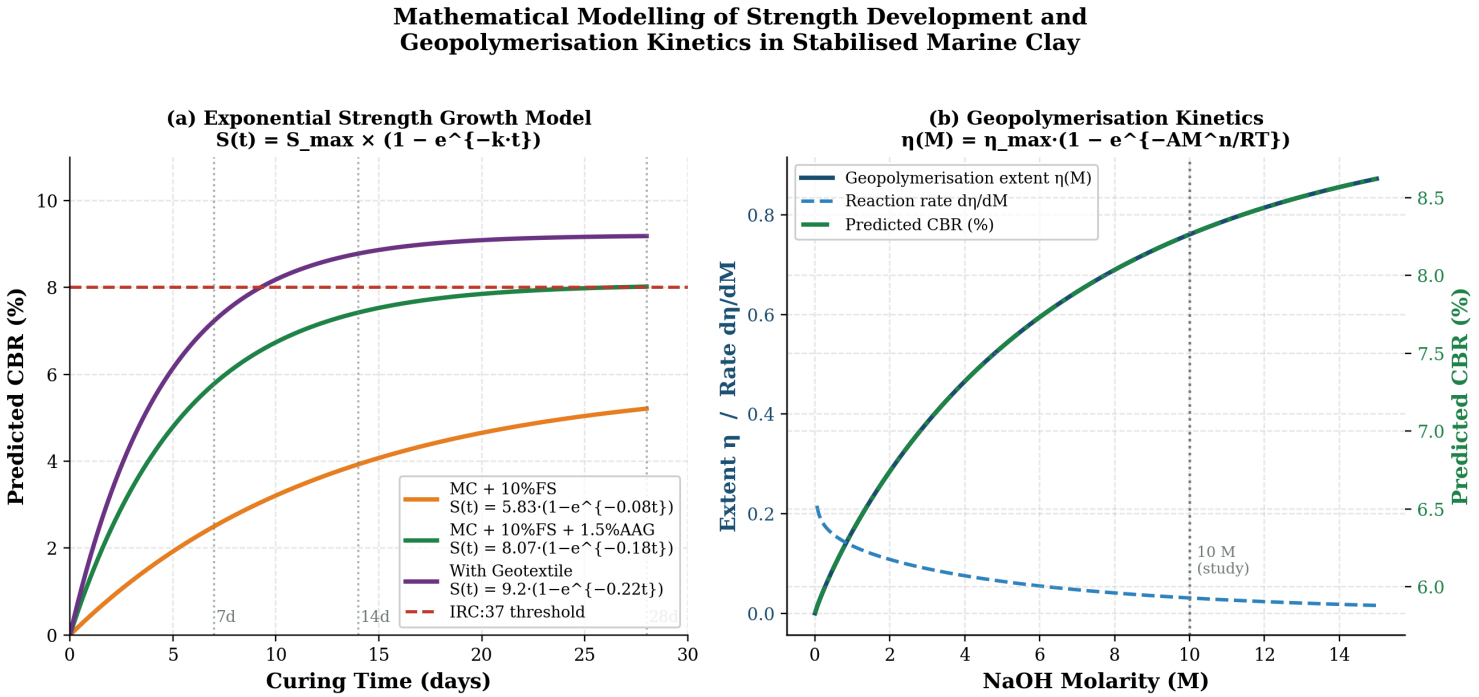


Figure 11

Mathematical models of strength development: (a) exponential growth model S(t) = S_max(1−e^{−kt}) for three treatment configurations; (b) Arrhenius-type geopolymerisation kinetics model η(M) and predicted CBR as functions of NaOH molarity.

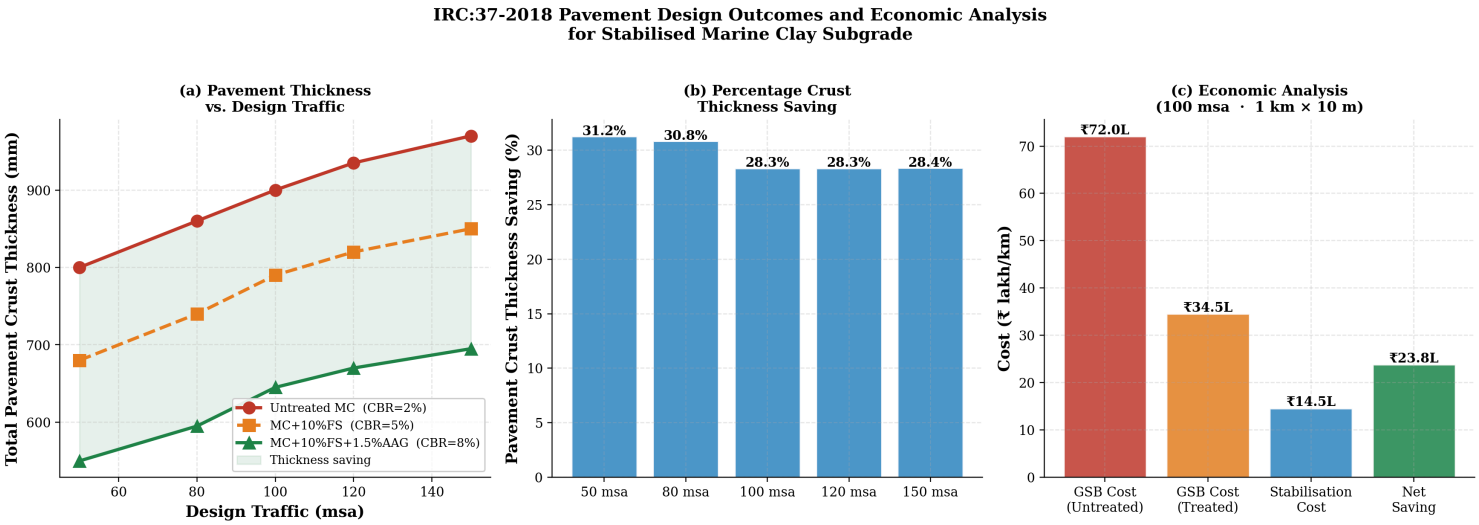


Figure 12

Pavement design and economic analysis: (a) total crust thickness vs. design traffic for three subgrade conditions; (b) percentage crust thickness saving for FS+AAG vs. untreated; (c) cost comparison at 100 msa (₹ lakh/km).

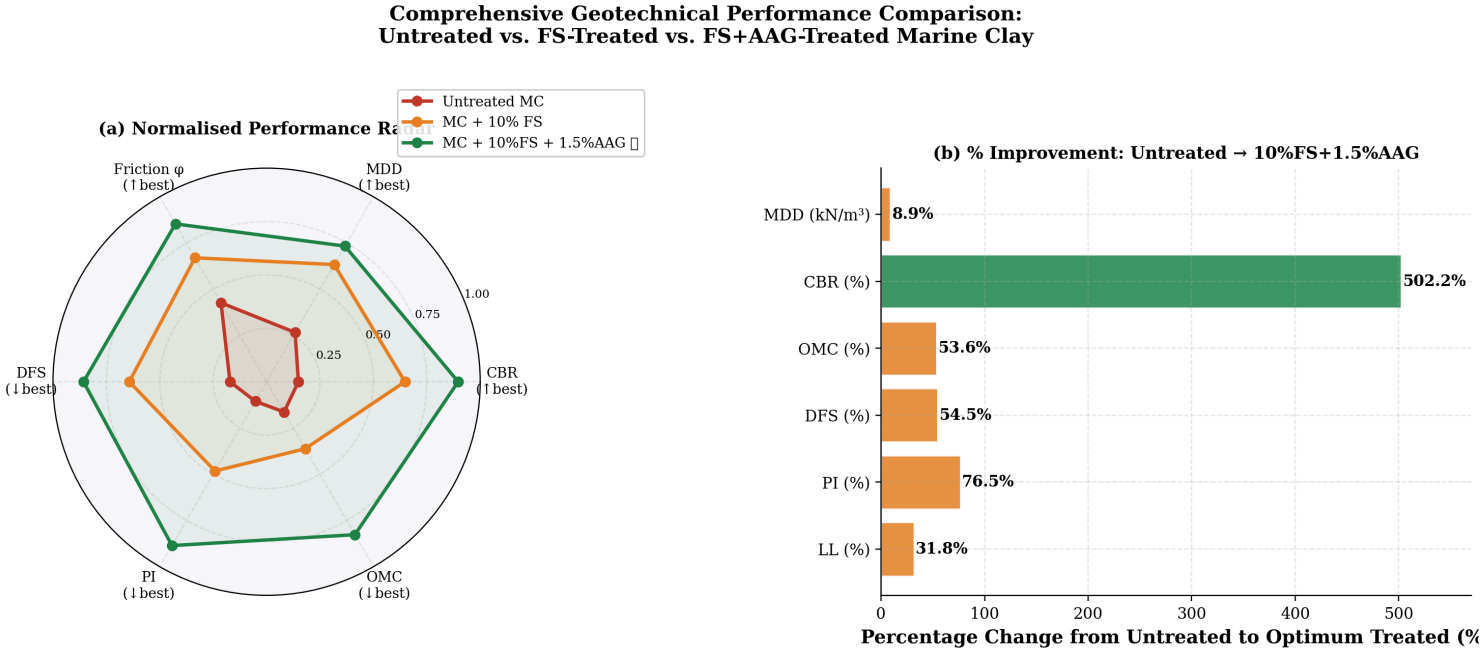


Figure 13

Comprehensive performance summary: (a) normalised radar chart comparing untreated, 10%FS-treated, and optimum 10%FS+1.5%AAG-treated marine clay across six normalised geotechnical parameters; (b) percentage improvement from untreated to optimum treatment.